Available online at www.sciencedirect.com
ScienceDirect
Journal of Power Sources 171 (2007) 373–380
JOURNAL OF POWER SOURCES
www.elsevier.com/locate/jpowsour

Methanol oxidation reaction on Ti/$RuO_{2(x)}Pt_{(1-x)}$ electrodes prepared by the polymeric precursor method

R.G. Freitas [a], L.F. Marchesi [a], R.T.S. Oliveira [a,b,d], F.I. Mattos-Costa [a], E.C. Pereira [a], L.O.S. Bulhões [a,c], M.C. Santos [a,d,*]

[a] *Laboratório Interdisciplinar de Eletroquímica e Cerâmica, Centro Multidisciplinar para o Desenvolvimento de Materiais Cerâmicos, Departamento de Química, Universidade Federal de São Carlos, Caixa Postal 676, 13560-905 São Carlos, SP, Brazil*
[b] *Grupo de Materiais Eletroquímicos e Métodos Eletroanalíticos, Instituto de Química de São Carlos, Universidade de São Paulo, Caixa Postal 780, 13566-590 São Carlos, SP, Brazil*
[c] *CENIP, Centro Universitário Central Paulista, UNICEP, Rua Miguel Petroni, 5111, CEP 13563-470, São Carlos, SP, Brazil*
[d] *LEMN, Laboratório de Eletroquímica e Materiais Nanoestruturados, CCNH-Centro de Ciências Naturais e Humanas, UFABC-Universidade Federal do ABC, CEP 09.210-170, Rua Santa Adélia 166, Bairro Bangu, Santo André, SP, Brazil*

Received 12 March 2007; received in revised form 23 May 2007; accepted 4 June 2007
Available online 23 June 2007

Abstract

In this work, ruthenium oxide films containing platinum nanoparticles were prepared using the polymeric precursor method on Ti substrates with several molar ratios. This paper aims at presenting the characterization of the Pt content effect in the methanol electrochemical oxidation reaction. The films were physically characterized using X-ray diffraction and both Pt and RuO_2 (rutile) phases were observed. The mean crystallite sizes were 6 nm for Pt and 25 nm for RuO_2. The X-ray photoelectronic results indicated that on the electrodes surfaces, depending on the substrate, there was RuO_2, Ru metal and Pt metal. Besides, it was not observed the formation of PtRu alloys. The atomic force microscopy images of the films showed highly rough surfaces. A decrease in the roughness mean square values is observed as the Pt content increases. These last results are similar to electroactive surface area values calculated by redox-couple (K_4FeCN_6/K_3FeCN_6). There was an increase in the globular size observed on the electrode surface and lower particle dispersion as the Pt content is increased from 12.5 to 75 mol%. Regarding the eletrode electrocatalytical behavior for methanol oxidation, it was observed that the onset oxidation overpotential is displaced towards more negative values as Pt content is decreased. Besides, an increase has been shown in the current density for methanol oxidation of 600% using a Ti/RuO_2-Pt (87.5:12.5) electrode compared to polycrystalline Pt.

Keywords: Methanol oxidation reaction; Electrocatalysis; Pt nanoparticles; Polymeric precursor method

1. Introduction

Direct methanol fuel cells, DMFC, are proposed as portable power source. One of the most important problems in these devices is the low reactivity for methanol oxidation at low temperatures [1]. Nowadays, binary PtRu alloys are recognized as the best electrocatalysts for this reaction. Literature data show that the electrocatalytical activity of Pt for the methanol electrochemical oxidation reaction can be improved adding other metals as alloying elements, such as Ru [2], Sn [3] and Rh [4]. This alternative aims to decreasing the Pt surface poisoning by the strongly bonded intermediates, such as CO. On the other hand, recent studies revealed that hydrated ruthenium dioxide ($RuO_2{\cdot}xH_2O$) is a more active electrocatalyst for this reaction [5–10] than the bimetallic PtRu alloy [11]. Additionally, it has been shown that RuO_2-Pt electrocatalysts are very promising composite materials to be used in fuel cell anodes.

In general, RuO_2-Pt electrocatalysts for methanol oxidation reaction are synthesized using sol–gel route [5,6,9,10], thermal decomposition [7] and a two-step process [1]. In these cases a mixture of RuO_2 and Pt nanoparticles is obtained. Important

* Corresponding author at: LEMN, Laboratório de Eletroquímica e Materiais Nanoestruturados, CCNH-Centro de Ciências Naturais e Humanas, UFABC-Universidade Federal do ABC, CEP 09.210-170, Rua Santa Adélia 166, Bairro Bangu, Santo Andreĭ, SP, Brazil. Tel.: +55 11 4437 1600; fax: +55 11 4437 1600.
E-mail address: mauro.santos@ufabc.edu.br (M.C. Santos).

0378-7753/$ – see front matter © 2007 Elsevier B.V. All rights reserved.
doi:10.1016/j.jpowsour.2007.06.046

effects on the methanol oxidation reaction were observed using these films. Such effects are associated with the presence of RuOH bonds [12] at the RuO_2 surface, following the well-known bifunctional mechanism [13,14]. In this mechanism, RuOH promotes the oxidation of the strongly bonded CO_{ads} residues on Pt, due to the presence of hydroxyl species adjacent to the Pt–CO_{ads} sites.

In order to explore the eletrocatalytical properties of RuO_2-Pt electrodes for methanol oxidation, new strategies of synthesis to prepare these materials are proposed [1,5–7]. Recently, a study using the polymeric precursor method, PPM, to prepare Pt electrodes has been published [15]. These electrodes were tested for methanol and ethanol oxidation [16] showing an increase in the current densities of 934 and 440%, respectively, compared with polycrystalline Pt. Furthermore, there is only one work concerning the polymeric precursor method (PPM) fabrication of RuO_2-Pt thin films [17]. That work described the preparation and characterization of RuO_2-Pt catalysts in the form of powder or supported on carbon powder (Vulcan XC72) substrate for methanol oxidation in a direct methanol fuel cell (DMFC). The results indicated a low power density, but the thermal decomposition of polymeric precursors seems to be a promising method to prepare catalysts supported on carbon powder that can be applied to these systems. In another paper, Ti/RuO_2-Pt anodes with a varying Ru:Pt ratio were prepared by thermal deposition of a RuO_2-Pt catalyst layer onto a Ti mesh for DMFC [18]. The results showed that these electrodes were very active for the methanol oxidation and that the optimum Ru surface coverage was ca. 38% for a DMFC operating at 20–60 °C.

In the present paper, thin films of RuO_2-Pt were prepared using the PPM and deposited over Ti substrates. These films were characterized by X-ray diffraction, XRD, atomic force microscopy, AFM, and cyclic voltammetry, CV techniques. The film electroactive surface areas, ESA, were measured using a redox-couple (K_4FeCN_6/K_3FeCN_6). The electrocatalytical activity for methanol oxidation reaction was evaluated by CV and chronoamperometric, CA measurements. The proposal of this work is to decrease the platinum content in the electrocatalyst without any loss of the electrode electrocatalytical activity toward methanol oxidation reaction. In this sense, we used Pt contents between 75 and 12.5 mol% in RuO_2 electrodes.

2. Experimental

2.1. Electrode preparation

The electrodes were prepared using a titanium plate (geometric area = 1 cm^2) as substrate (TiBrasil 99.7%). The substrates were treated by sandblasting followed by a chemical treatment in hot aqueous oxalic acid 10% (w/w) for 30 min. After the chemical treatment, the substrates were washed with Millie-Q water and dried at 130 °C.

The precursor solution was prepared dissolving citric acid, CA (Synth) in ethylene glycol, EG (Merck) using 1:4.65 ratio at 60 °C. In this solution, different amounts of $H_2PtCl_6{\cdot}7H_2O$ (Aldrich) and $RuCl_3{\cdot}3H_2O$ (Aldrich) were added maintaining the total metal amount constant in the following ratio: 1:62.5:290.6 (metal:CA:EG). Different Pt contents were used to prepare the Ti/$RuO_{2(x)}Pt_{(1-x)}$ electrodes where the ratio in mol% among RuO_2 and Pt amounts were: (100:0), (87.5/12.5), (75:25), (50:50) and (25:75).

The precursor solution was painted with a brush onto the support (Ti) and the material was initially treated at 130 °C for 10 min to eliminate water, 250 °C for 20 min and 400 °C for 30 min to eliminate the organic materials producing the composite films. This procedure was repeated ten times and, at the end, the electrode mass was close to 0.1 mg cm^{-2}. After the last thermal treatment, the electrode was cooled using 5 °C min^{-1} until room temperature. All electrodes were fabricated in static air atmosphere.

2.2. Electrodes characterization

The electrochemical characterization was accomplished using a potentiostat/galvanostat EG&G PARC model 263A. All the electrochemical experiments were carried out at 25 °C. The voltammetric curves were measured in a 0.1 mol L^{-1} $HClO_4$ solution in the potential range between 0.05 and 1.4 V (versus a reversible hydrogen electrode RHE). The methanol oxidation was investigated in a 0.1 mol L^{-1} $HClO_4$ solution containing 0.5 mol L^{-1} methanol by means of CV and CA. A Pt plate was used as auxiliary electrode (geometric area 3 cm^2). Prior to the experiments, the solutions were deaerated with N_2 for 30 min. The X-ray diffraction (XRD) patterns were obtained using a SIEMENS diffractometer model D-5000 with Cu Kα radiation and λ = 1.5406 Å. The AFM micrographs were obtained using a Molecular Imaging model PicoLe equipment. The X-ray photoelectron spectroscopy (XPS) analysis was performed using a Kratos Analytical XSAM HS spectrometer, with an Al Kα ($h\nu$ = 1486.6 eV) X-ray source. The binding energies were referred to the adventitious hydrocarbon C 1s line set at 284.8 eV. Gaussian line shapes were used to fit the curves for C 1s and O 1s, and a mixed Gaussian/Lorentzian function was employed for Pt 4f and Ru 3d. The Shirley background and a least-squares routine were used for fitting of the peaks. The sensitivity factors for quantitative analysis were referenced to SF 1s 1.0.

3. Results and discussion

3.1. Characterization of the Ti/RuO_2-Pt electrodes

3.1.1. X-ray diffraction analysis

X-ray diffraction patterns measured for Ti/RuO_2-Pt films with different Pt contents are presented in Fig. 1. The characteristic peaks of RuO_2 (JCPDS PDF#40-1290) rutile phase and Ti (PDF#44-1294) can be easily seen. Pt is evidenced at $2\theta = 46.24°$ (2 0 0) (JCPDS PDF#04-0802). The material microstructures here presented (peak patterns intensities) are different from the literature data [17] using the same preparation method but deposited on carbon. This can be attributed to the presence of Pt and Ru in small amounts in this paper compared to that paper [17]. The mean crystallite size calculated for Pt and RuO_2 were estimated using the Scherrer equation [19] and the software Winfit 1.2 [20], at the crystalline planes ((2 0 0): $2\theta = 46.24°$) and

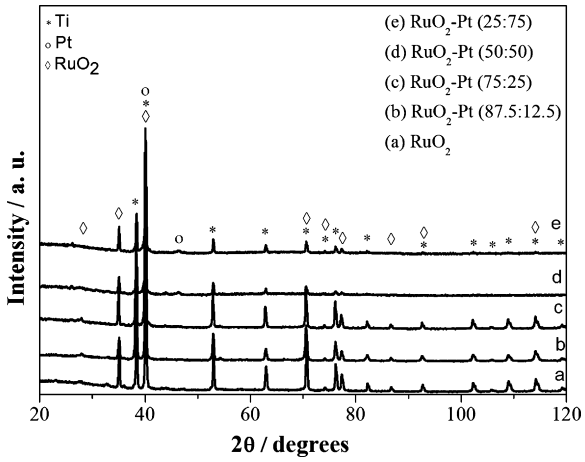

Fig. 1. X-ray diffraction patterns for Ti/RuO_2-Pt films obtained from the polymeric precursor method.

((1 0 1): $2\theta = 35.05^\circ$), respectively. These results are presented in Table 1.

In Table 1, it can be seen that the mean crystallite size for Pt is between 4 and 6 nm, and for RuO_2 it is close to 25 nm. These results for Pt are similar to those found for the samples prepared using a sol–gel procedure [5,6], but they are different, if compared to the paper of Profeti et al. [17] which used PPM to fabricate their samples. It is well known that composition changes in the precursor polymer can lead to important differences in the phase quantity and lattice defects for oxides prepared using the PPM [21,22]. For this reason, the mean crystallite sizes in that paper, Profeti et al. [17] (1:4:16 (metal:CA:EG)) are different from those ones here presented for a much more diluted metal salt composition (1:62.5:290.6 (metal:CA:EG)).

3.1.2. X-ray photoelectronic spectroscopy

XPS analyses were carried out on as-prepared samples. Widerange XP spectra lead to conclude that the surfaces were free from contamination with Ti (from the substrate) or chloride (from the solutions). The features for detailed scans were recorded for the Pt 4f, Ru 3d, O 1s, and C 1s regions. For clarity were presented only three samples, but the measurements were performed for all samples. Fig. 2a shows the Ru 3d + C 1s spectra for a Ti/RuO_2 electrode (100% RuO_2). The spectrum was deconvoluted into three components with binding energies of 280.18, 280.90, and 284.5 eV. The line that has its major intensity occurs at 280.18 eV and it can be associated to metallic Ru [23,24]. The binding energy of 280.90 eV can be attributed to RuO_2 component and the photoelectron intensity above 284 eV corresponds to Ru–O speciation [23]. By comparing the photoelectron spectra of Fig. 2a and b (Ru 3d + C 1s high-resolution XP spectra for Ti/RuO_2Pt electrode (RuO_2Pt, 75/25)), it becomes quite clear that the components of the XP spectrum of the Ti/RuO_2 (100% RuO_2 sample) (Fig. 2a) can be associated to both ruthenium oxides and metallic ruthenium in the zero-valence state. In fact, this is surprising since published results using the sol–gel route for RuO_2 and RuO_2Pt electrodes has been shown no Ru metal [5]. However, using the PPM method is common to obtain metals in zero-valence state [15,16]. The binding energies of 280.9 eV (3d5/2) and 284.5 eV (3d3/2) were attributed to RuO_2 [5,24]. It is important to stress that this work shows that Ru 3d spectra obtained for all Ti/RuO_2Pt electrodes used in all compositions (examples see Fig. 2a and b), proves the presence in the near-surface of ruthenium in the zero-valence state and the presence of RuO_2, therefore, indicates that no Pt–Ru alloy is present in the Ti/RuO_2 or Ti/RuO_2Pt electrodes, in agreement with the XRD data.

Table 1
Mean crystallite size for Ti/RuO2-Pt electrodes prepared by the polymeric precursor method

Composition	Mean crystalline size (nm)	
	Pt	RuO_2
RuO_2	–	27
RuO_2/Pt (25:75)	4	26
RuO_2/Pt (50:50)	6	27
RuO_2/Pt (75:25)	4	25
RuO_2/Pt (87.5:12.5)	–	22

The Pt 4f XP spectrum for the Ti/RuO_2Pt electrode (RuO_2Pt, 75/25) is presented in Fig. 2c. The spectrum was deconvoluted into three doublets with binding energies of 71.15, 73.5, and 74.5 eV. The line with major intensity centered at 71.15 eV can be assigned to Pt in the zero-valence metallic state [23]. The peak components at 73.5 and 74.5 eV can be attributed to Pt^{2+} and Pt^{4+} species [23]. The O 1s photoelectron spectrum for the Ti/RuO_2Pt sample (not shown) was composed of species with binding energies that can be attributed to oxide oxygen (530.1 eV, typical value of transition metal oxides) and to hydroxides (531.6 eV) [25]. Concerning the RuO_2/Pt ratio for all compositions, a Pt surface enrichment (10–15% higher than the nominal composition of the resin) was observed.

3.1.3. Atomic force microscopy

Fig. 3 shows the atomic force microscopy images of the six electrode surfaces. The Pt and Ti substrates micrographs are also presented in Fig. 3 to show the globular evolution of the film morphology as the Pt content on RuO_2 increases. The images in Fig. 3 show that all the surfaces are rough, which is expected for RuO_2-Pt thin films [9]. Comparing the RuO_2-Pt samples, a change is observed in electrode surface globular characteristic as the Pt content changes. Also, a decrease is observed in the roughness mean square, RMS, as the Pt content is increased (Table 2). The last value is similar to the one related to Ti substrate (611.62 nm).

3.1.4. Electrochemical characterization

The electroactive surface area ESA for Pt–Ru alloys are, in general, calculated using the oxidation charge of one CO_{ads} monolayer [26]. However, this procedure should not be made in this work, since on RuO_2 sites there is no CO adsorption, as proved previously using EQCN technique [37]. For RuO_2-Pt electrodes, to our knowledge, no paper has been published concerning the calculation of the ESA. For this reason, in this paper we propose to use the redox-couple (K_4FeCN_6/K_3FeCN_6) to calculate this parameter for the investigated samples. This

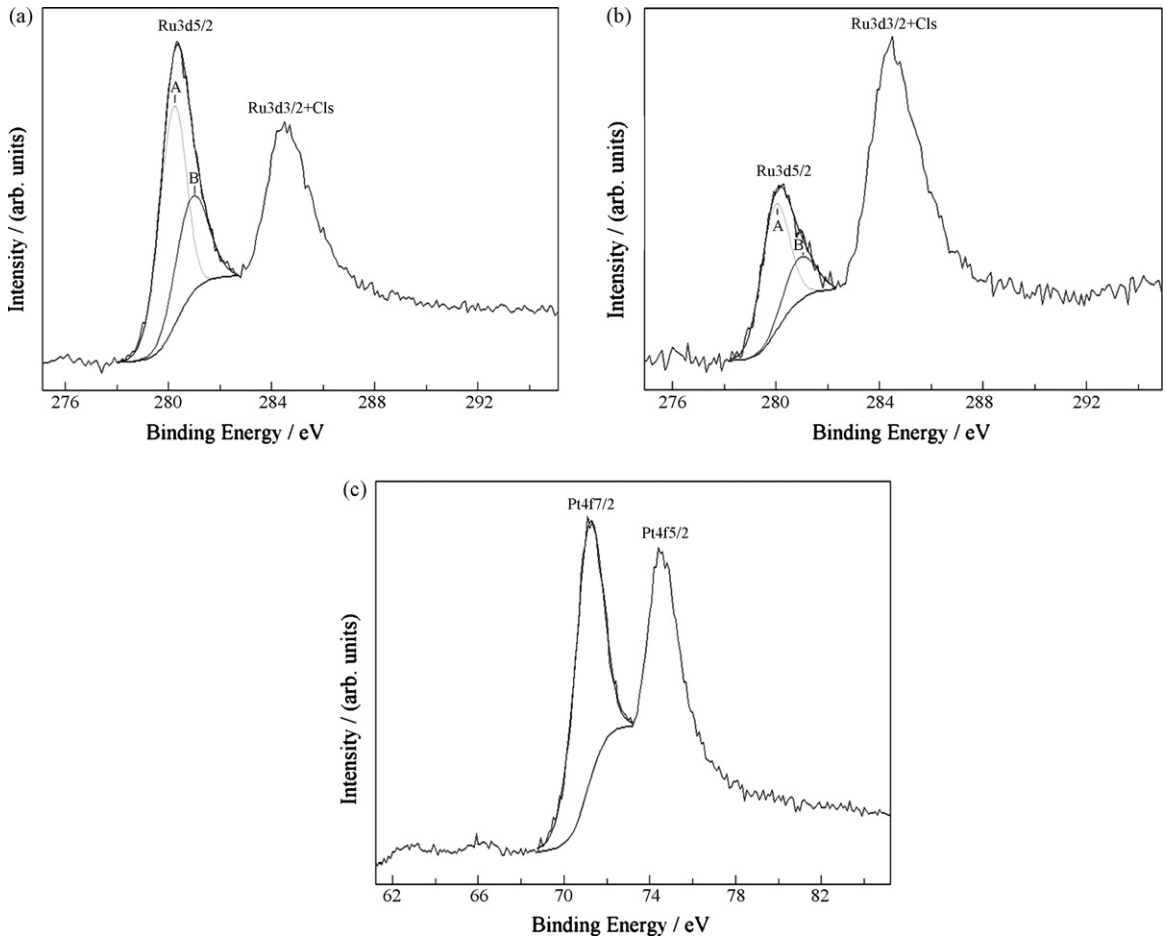

Fig. 2. (a) Ru 3d + C 1s high-resolution XP spectra for Ti/RuO_2 electrode (100% RuO_2), (b) Ru 3d + C 1s high-resolution XP spectra for Ti/RuO_2Pt electrode (RuO_2Pt, 75/25), (for clarity, only the fits for Ru 3d5/2 lines are shown). (c) Pt 4f high-resolution XP spectra for Ti/RuO_2Pt electrode (RuO_2Pt, 75/25). Only fits for Pt 4f7/2 lines are shown, for clarity.

methodology was described before for the calculation of ESA in both boron-doped diamond, BDD, electrodes and BDD electrodes covered with RuO_2-Pt thin films [27,28]. The ESA of the modified electrodes was roughly estimated using this methodology. There, the voltammetric peak current measured for the different surfaces using a typical outer-sphere and diffusion-controlled reaction, such the $K_4Fe(CN)_6/K_3Fe(CN)_6$ redox-couple in solution were compared with that of a polycrystalline Pt electrode whose area was previously calculated using the H-adsorption/desorption charge density in a $HClO_4$ solution. This procedure was performed to exclude the possibility that the enhancement observed in the oxidation currents could be due to surface roughness changes, i.e., an area effect and not to a real electrocatalytic effect.

The equation to calculate the ESA of the RuO_2-Pt and RuO_2 is:

$$A_{\text{electrode}} = A_{\text{Pt}} \times \frac{I(FeCN_6{}^{3-}/FeCN_6{}^{4-})_{\text{electrode}}}{I(FeCN_6{}^{3-}/FeCN_6{}^{4-})_{\text{Pt}}} \quad (1)$$

With the current peak for the reduction of $FeCN_6{}^{3-}$ in all electrodes it was possible to obtain the ESAs which are presented in Table 3. It is observed that RuO_2 presents a roughness factor of 9. The binary systems RuO_2-Pt presented similar ESA. All the subsequent electrochemical experiments were normalized using the ESA of the electrodes.

The voltammetric profiles in acidic medium of the thin film electrodes prepared with different compositions are presented in Fig. 4. The voltammetric profile shown in Fig. 4 is similar to

Table 2
Roughness mean square of the Ti/RuO2Pt electrodes compared to bare Pt

Composition	RuO_2	RuO_2/Pt (87.5/12.5)	RuO_2/Pt (75/25)	RuO_2/Pt (50/50)	RuO_2/Pt (25/75)	Pt
RMS	850	850	970	780	600	7.441
	858.89	800	980	700	630	7.227
RMS_{mean} (nm)	854.44 ± 6.2	825 ± 35.3	975 ± 7.0	740 ± 56.5	615 ± 21.2	7.334 ± 0.15

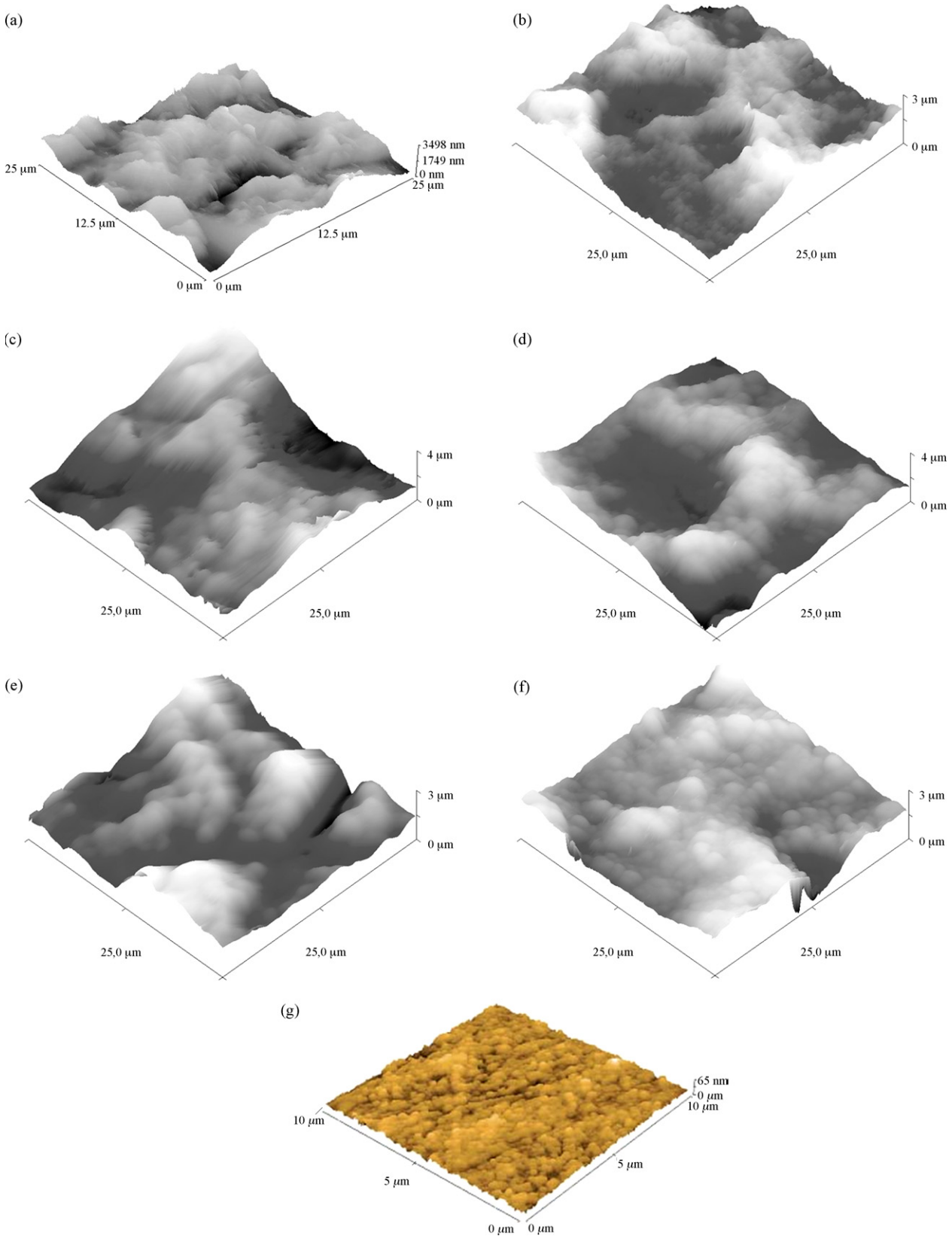

Fig. 3. Tri-dimensional AFM images of the substrates: (a) Ti, (b) RuO_2, (c) RuO_2/Pt (87.5/12.5), (d) RuO_2/Pt (75:25), (e) RuO_2/Pt (50:50), (f) RuO_2/Pt (25:75) and (g) polycrystalline Pt.

Table 3
Electroactive surface areas and roughness factors obtained by comparative cyclic voltammetries with a platinum electrode in 1 mol L^{-1} $K_4Fe(CN)_6$ + 0.1 mol L^{-1} $HClO_4$

Electrode material	Geometric area (cm^2)	Electroactive surface area (cm^2)	Roughness factor
RuO_2	1	9	9
RuO_2/Pt (25/75)	1	11	11
RuO_2/Pt (50/50)	1	11	11
RuO_2/Pt (75/25)	1	12	12
RuO_2/Pt (87.5/12.5)	1	12	12

those presented in the literature for RuO_2 [29–31] and RuO_2-Pt films [5,6,9,12]. Dobholfer et al. [32] proposed that RuO_2 electrodes present redox transitions between Ru^{2+} to Ru^{6+} in the potential range between 0.4 and 1.4 V (versus RHE) in acidic medium. For this reason, the voltammetric profile between 0.4 and 1.4 V can be associated with the following redox transitions:

$$RuO{\cdot}xH_2O \rightarrow RuO(OH)(x-y)H_2O + 2H_2O + 1e^- + H^+ \quad (2)$$

$$RuO(OH)(x-y)H_2O \rightarrow RuO_2{\cdot}(x-y)(H_2O) + H^+ + 1e^- \quad (3)$$

$$RuO_2{\cdot}(x-y)H_2O \rightarrow RuO_3 + zOH^- + (z+2)H^+ + 2e^- \quad (4)$$

proposed using electrochemical quartz crystal nanobalance technique [12], where there is a double injection mechanism of protons and electrons during oxidation/reduction cycles for RuO_2.

Still analyzing Fig. 4, it can be seen that as there is an increase on the Pt content in the electrocatalyst there is a decrease in the capacitive currents between 0.4 and 1.4 V. These results are in agreement with previous works published using the sol–gel [5,6,33] and PPM [17]. From a different point of view, the RuO_2-Pt (75:25) presents the voltammetric shape of a polycrystalline Pt electrode. The characteristic redox process can be observed in Fig. 4 for this sample: (i) adsorption and desorption of hydrogen

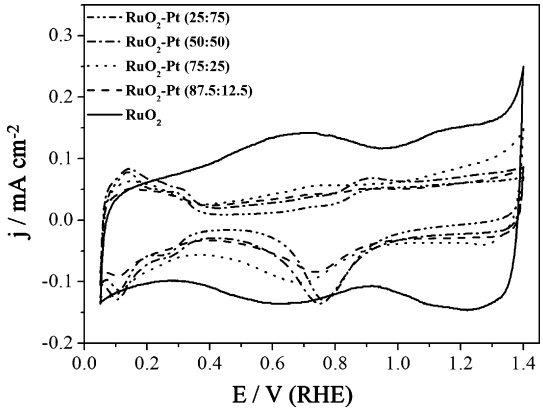

Fig. 4. Cyclic voltamograms of Ti/RuO_2-Pt characterization of the electrodes in 0.1 mol L^{-1} $HClO_4$, sweep rate = 50 mV s^{-1}, T = 25 °C.

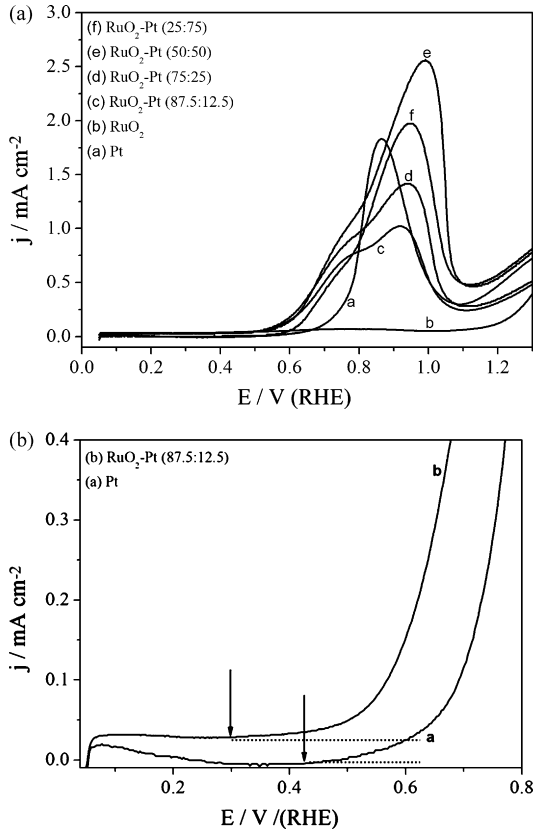

Fig. 5. (a) Cyclic voltamograms for methanol oxidation (0.5 mol L^{-1}) in 0.1 mol L^{-1} $HClO_4$, sweep rate = 50 mV s^{-1} on the different electrodes as described in the figure. (b) Cyclic voltamograms for methanol oxidation (0.5 mol L^{-1}) in 0.1 mol L^{-1} $HClO_4$, sweep rate = 50 mV s^{-1}. (a) Pt and (b) Ti/RuO_2-Pt (87.5:12.5).

UPD on Pt (0.05 e 0.4 V), (ii) anions adsorption in the double layer region (0.4 and 0.9 V) and formation a reduction of the superficial PtO, between (0.9 and 1.4 V) and (1.4 and 0.5 V).

3.2. Electrocatalytical activity of the electrodes toward methanol oxidation

The electrocatalytical activity of the different materials was evaluated using CV as shown in Fig. 5a. For metallic Pt, it is observed the typical behavior of methanol oxidation [34] (presence of two peaks at 0.85 and 1.25 V) related to methanol oxidation from strongly bonded adsorbed intermediates as CO_{ads} and the oxidation of byproducts produced during the methanol oxidation, formic acid and formaldehyde, respectively, in a scan toward positive direction between 0.05 and 1.55 V.

For pure RuO_2 the electrocatalytical activity for methanol oxidation is in agreement with literature [35–37]. It is suggested here that this behavior is due to the non-adsorption of strongly bonded intermediates as CO_{ads}, which is confirmed by the use of the electrochemical quartz crystal nanobalance technique [37].

As the Pt content is increased, an enhancement is observed in electrocatalytical activity compared to pure Pt. For the smallest Pt content (12.5%), the onset potential for methanol oxidation is shifted 130 mV towards more negative potentials compared to polycrystalline Pt (Fig. 5b). However, the peak potential

(compared to metallic Pt) is displaced in the positive potential direction by 110 mV for RuO_2-Pt (50:50). Two important characteristics should be pointed out:

(1) There is an increase in the current densities for methanol oxidation (at 1 V) as the Pt content increases up to RuO_2-Pt (50:50). This effect is probably related to the bifunctional mechanism, where an equal number of Pt–CO_{ads} sites and $RuO(OH)(x-y)H_2O$ react to form CO_2. For the highest Pt composition in the film (RuO_2-Pt (25:75)) there is a decrease in the peak current density for methanol oxidation compared to the same data for (RuO_2-Pt (50:50)), which probably is related to an increase of presence of strong adsorbed species, such as CO_{ads}, on Pt sites.
(2) There is a pre-peak between 0.7 and 0.8 V, which has not been observed on Pt. This peak has already been observed in literature [7] describing the oxidation of methanol on RuO_2 films with dispersed Pt nanoparticles. The presence of this peak could be associated with a change in the mechanism reaction for methanol oxidation, but further work must be performed using spectroscopic techniques to identify the produced species in that potential region.

It is important to stress that the current values were normalized by the ESA of the electrodes which indicates that the electrocatalytical behavior observed in the voltammetric experiments (Fig. 5a and b) could be explained by: (i) a better Pt dispersion on RuO_2 matrix with lower Pt contents (RuO_2-Pt, 87.5:12.5), (ii) a better distribution of RuO_2 in the adjacent Pt sites which increases the bifunctional mechanism, (iii) an increase of Pt activity associated with electronic effects and (iv) a non-adsorption of CO_{ads} on RuO_2 as suggested in reference [37] which leads to an enhancement of methanol oxidation by the bifunctional mechanism. In general, the electrocatalytical action of the different RuO_2 films containing dispersed Pt nanoparticles on methanol oxidation is a synergic effect as proposed before [17].

The only work in the literature using the same methodology to the preparation of RuO_2 containing Pt nanoparticles [17] described that the general characteristic of the electrodes is that they have similar behavior (for both the non-supported and those supported on high area carbon). According to the authors, this is confirmed by preliminary studies performed in a unitary fuel cell. In contrast, in the present paper, important differences were observed in the electrocatalytical behavior for methanol oxidation at different electrodes. The results here obtained do not imply that the Pt load cannot be minimized. A factorial design methodology can be carried out in order to make a trial of variables, such as temperature and resin composition to improve electrocatalytical performance for methanol oxidation decreasing, at the same time, the Pt content.

Chronoamperometric experiments for methanol oxidation at a constant potential (0.5 V) during 15 min (Fig. 6) were carried out. The best results were observed for the electrodes with the lowest Pt content. Analyzing Fig. 5 it is observed that the current density after 15 min is 12 $\mu A\,cm^{-2}$ for the RuO_2-Pt (87.5:12.5), which is 600% higher than the current density for methanol oxidation on polycrystalline Pt at the same potential. Then, it is evidenced that the lowest Pt content presents an enhanced electrocatalytical performance, which is desirable both in economical terms (a small load of Pt in the electrocatalyst) and because of the formation of nanoparticles with small sizes (in order to enhance the electrocatalytical behavior) (Fig. 6).

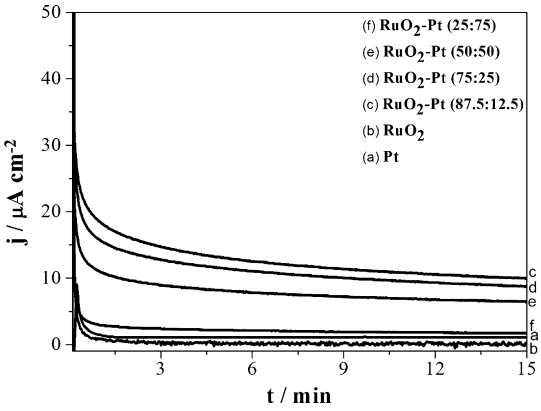

Fig. 6. Chronoamperometry for 0.5 mol L^{-1} methanol oxidation in 0.1 mol L^{-1} $HClO_4$. E_{ox} = 0.5 V. Different electrodes described in the figure.

With the results exposed above the best electrocatalytical performance for methanol oxidation was for RuO_2-Pt (87.5:12.5). The explanation for this behavior can be associated to a synergic effect of Pt and RuO_2 concerning different reasons: (i) a better Pt dispersion on RuO_2 matrix in the presence of small Pt load, (ii) a better distribution of RuO_2 in the adjacent sites of Pt particles which may increase the bifunctional mechanism [17], (iii) an enhancement in the electrocatalytical behavior of Pt by an electronic effect [17] and the non-CO_{ads} adsorption on the RuO_2 sites, as proved before using EQCN technique [37], which makes that the CO adsorbs only on Pt, liberating the RuO_2 sites to generates hydroxide species at low potentials in order to oxidize the species produced on the Pt surface.

4. Conclusions

In this work, RuO_2 films containing Pt nanoparticles were prepared, characterized and tested for methanol oxidation reaction. It was observed that the lowest load of Pt in the electrocatalyst RuO_2-Pt (87.5:12.5) promotes the highest enhancement in the electrocatalytical performance for methanol oxidation with a shift in the onset potential toward less positive values (by 130 mV) compared to Pt and an increase in the density current for methanol oxidation of 600% compared to Pt. The observed phenomenon is associated with a synergic effect of Pt nanoparticles and RuO_2 matrix, where different reasons for this should be pointed out: (i) a better Pt dispersion on RuO_2 matrix, (ii) a better RuO_2 distribution in Pt adjacent sites (which may increase the bifunctional mechanism), (iii) an enhancement in the electrocatalytical Pt nanoparticles performance for methanol oxidation (associated with an electronic effect) and (iv) a non-CO adsorption on RuO_2 sites, which liberates the RuO_2 sites to generate hydroxide species at low potentials (these species are responsible for the oxidation of the organic adsorbates on Pt).

Acknowledgements

The authors wish to thank the Brazilian Funding Institutions CNPq, CAPES, and FAPESP (Processes Numbers: 05/59992-6, 04/04869-2, 03/09933-8) for their financial support.

References

[1] Z. Chen, X. Qiu, B. Lu, S. Zhang, W. Zhu, L. Chen, Electrochem. Commun. 7 (2005) 593.
[2] L. Dubau, F. Hahn, C. Coutanceau, J.M. Léger, C. Lamy, J. Electroanal. Chem. 554 (2003) 407.
[3] C. Panja, N. Saliba, B.E. Koel, Surf. Sci. 395 (1998) 248.
[4] J.P.I. de Souza, S.L. Queiroz, K. Bergamaski, E.R. Gonzalez, F.C. Nart, J. Phys. Chem. B 106 (2002) 9825.
[5] H.M. Villullas, F.I. Mattos Costa, L.O.S. Bulhões, J. Phys. Chem. B 108 (2004) 12898.
[6] H.B. Suffredini, V. Tricoli, L.A. Avaca, N. Vatistas, Electrochem. Commun. 6 (2004) 1025.
[7] L.X. Yan, R.G. Allen, K. Scott, P.A. Christenson, S. Roy, Electrochim. Acta 50 (2005) 1217.
[8] Z. Chen, X. Qiu Lu Bin, S. Zhang, W. Zhu, L. Chen, Electrochem. Commun. 7 (2005) 593.
[9] G.R. Salazar-Banda, H.B. Suffredini, M.L. Calegaro, S.T. Tanimoto, L.A. Avaca, J. Power Sources 162 (2006) 9.
[10] H.M. Villullas, F.I. Mattos-Costa, P.A.P. Nascente, L.O.S. Bulhões, Chem. Mater. 18 (2006) 5563.
[11] J.W. Long, R.M. Stroud, K.E. Swider Lyons, D.R. Rolison, J. Phys. Chem. B 104 (2000) 9772.
[12] M.C. Santos, A.J. Terezo, V.C. Fernandes, E.C. Pereira, L.O.S. Bulhões, J. Solid State Electrochem. 9 (2005) 91.
[13] M. Watanabe, S. Motoo, J. Electroanal. Chem. 60 (1975) 267.
[14] H.A. Gasteiger, N. Markovic, P.N. Ross, E.J. Cairns, Electrochim. Acta 39 (1994) 1825.
[15] R.G. Freitas, R.T.S. Oliveira, M.C. Santos, L.O.S. Bulhões, E.C. Pereira, Mater. Lett. 60 (2006) 1906.
[16] R.G. Freitas, M.C. Santos, R.T.S. Oliveira, L.O.S. Bulhoes, E.C. Pereira, J. Power Sources 158 (2006) 164.
[17] L.P.R. Profeti, F.C. Simões, P. Olivi, K.B. Kokoh, C. Coutanceau, J.-M. Léger, C. Lamy, J. Power Sources 158 (2006) 1195.
[18] Z.G. Shao, F.Y. Zhu, W.F. Lin, P.A. Christensen, H.M. Zhang, J. Power Sources 161 (2006) 813.
[19] B.D. Cullity, Elements of X-ray Diffaction, third ed., Addison-Wesley, Massachusetts, 1967, p. 262.
[20] www.geol.uni-erlangen.de.
[21] A.J. Terezo, E.C. Pereira, Electrochim. Acta 45 (2000) 4351.
[22] A.V. Rosario, E.C. Pereira, Sol. Energy Mater. Sol. Cells 71 (2002) 41.
[23] J.F. Moulder, W.F. Stikle, P.E. Sobol, K.D. Bomben, Handbook of X-ray Photoelectron Spectroscopy, Perkin-Elmer, 1992.
[24] D. Briggs, M.P. Seah, Practical Surface Analysis, vol.1, second edition, John Willey & Sons., 1993.
[25] I.M. Kodintsevt, S. Trasatti, M. Rubelt, A. Wieckowski, N. Kaufher, Langmuir 8 (1992) 283.
[26] G.A. Camara, R.B. de Lima, T. Iwasita, J. Electroanal. Chem. 585 (2005) 128.
[27] H.B. Suffredini, S.A.S. Machado, L.A. Avaca, J. Braz. Chem. Soc. 15 (2004) 16.
[28] H.B. Suffredini, V.A. Pedrosa, L. Codognoto, S.A.S. Machado, R.C. Rocha Filho, L.A. Avaca, Electrochim. Acta 49 (2004) 4021.
[29] S. Ardizzone, G. Fregonara, S. Trasatti, Electrochim. Acta 35 (1990) 263.
[30] A.J. Terezo, E.C. Pereira, Mater. Lett. 53 (2002) 339.
[31] S. Trasatti, G. Lodi, in: S. Trasatti (Ed.), Electrodes of Conductive Metallic Oxides, Part A, Elsevier, New York, 1980, p. 334.
[32] K. Dobholfer, M. Metikos, Z. Ogumi, H. Gerisher, Ber. Bunsenges Phys. Chem. 82 (1978) 1046.
[33] H. Mercedes Villullas, I.M.-C. Flora, O.S.B. Luis, J. Electroanal. Chem. 545 (2003) 89.
[34] T. Iwasita, Electrochim. Acta 47 (2002) 3663.
[35] L.D. Burke, O.J. Murphy, J. Electroanal. Chem. 101 (1979) 351.
[36] C.H. Lee, S.E. Bae, C.W. Lee, D.H. Jung, C.S. Kim, D.R. Shin, J. Hydrogen Energy 26 (2001) 175.
[37] M.C. Santos, L. Cogo, S.T. Tanimoto, M.L. Calegaro, L.O.S. Bulhões, Appl. Surf. Sci. 253 (2006) 1817.